# Optic Flow: Improving Discontinuity Preserving

N. Monzón López, J. Sánchez, and A. Salgado de la Nuez

Centro de Tecnologías de la Imagen
Departamento de Informática y Sistemas
Universidad de Las Palmas de Gran Canaria
nmonzon@ctim.es,{jsanchez,asalgado}@dis.ulpgc.es

**Abstract.** The aim of this paper is to analyze the discontinuity preserving behavior of two methods in optical flow. With this objetive, we have implemented a well-known optical flow method that uses isotropic TV-$L^1$ regularization. For the second approach, we have modified this method, by adding a decreasing function in the regularization term, to avoid smoothing at flow discontinuities. As a consequence, we see a high improvement and a very accurate discontinuities detection in some sequences but not good enough in others. Adapting the weight of the decreasing function allows us to better define the flow discontinuities. Nevertheless, the experimental results show that the parameters that yield a good segmentation of the motion field, may also introduce important unstabilities. In this sense, the results seem promising, but it is very difficult to set a unified parameter configuration that works fine for all the sequences. We evaluate the performance of these approaches with some standard test sequences, such as the Middlebury benchmark database or the Yosemite sequence. Looking for the best parameters configuration, which provides the best contour definition, does not typically mean a solution which is closer to the ground truth.

**Keywords:** Optical Flow, Discontinuity Preserving, TV-$L^1$, Variational Methods, Isotropic Regularization.

## 1 Introduction

The estimation of optical flow is one of the fundamental challenges in computer vision, which consists in estimating the apparent displacement of the pixels through an image sequence. Although there are several approximations to calculate the optical flow, the variational methods have proven to be among the most accurate methods in the literature [2].

There are still some limitations in current variational methods like, for instance, occlusions handling, that arise when a portion of the image is visible at one frame but not in its succesive, the estimation of large displacements or the preservation of discontinuities in the displacement field. This last topic has been a major theme in optical flow studies during the last years and is the basis for our work.

In 1981, Horn and Schunck [4] proposed which is considered the classical method in variational optical flow solutions, exposing a model to compute the

R. Moreno-Díaz et al. (Eds.): EUROCAST 2013, Part II, LNCS 8112, pp. 117–124, 2013.

flow field of an image sequence by calculating the flow as a minimization problem. Although their proposal was a breakthrough in the computer vision techniques, it still had limitations, highlighting that, in many situations, the mere gray value do not provide enough information to completely determine the motion field. One of these limitations is not dealing correctly with discontinuities in the displacement field.

Many authors have proposed improvements to the classical model in order to cope with motion discontinuities. Typically, many methods use anisotropic diffusion approaches provided that flow contours often appear in conjunction with high image gradients. For instance, in 1986 Nagel and Enkelmann [5] developed a new contribution to the literature introducing a new anisotropic diffusion operator that allows respecting the object boundaries during the diffusion process.

In 1990, Perona and Malik [6] contributed with a new definition of scale-space in computer vision, introducing a technique that realizes it using an anisotropic diffusion process reducing the image noise without removing significant parts of the image content. This approach was later used in the field of optical flow by Alvarez *et al.* [1]. Their work presented a new variational model that preserves discontinuities of the flow better than the classical approach.

Later, in 2004, Brox *et al.* [3] exposed a variational model which is more robust to the presence of outliers, generalizing the use of continuous $L^1$ functionals. This method has, among its main features, the ability to cope with constant brightness changes. Another optical flow estimation method was the anisotropic model introduced in Zach *et al.* [10] in 2007, which is based on the minimization of a functional containing a data term, using the pure $L^1$ norm, and a regularization term using the total variation of the flow. In Wedel *et al.* [8], this method was improved with the use of an anisotropic regularization induced by a strictly decreasing function. This function is utilized to inhibit the smoothing in the image areas in where the gradient is strong. Although this is an interesting idea and it has been used in some other works, like in [9], it has not been deeply studied yet.

Sánchez *et al.* [7] conducted a thorough analysis of the variational model presented in [3], using its own implementation, on some typical test sequences like Middlebury benchmark database or Yosemite. The source code can be downloaded here. In this work, the authors expose the major drawbacks of the method, especially the effect of creating rounding effects at the flow edges. The authors proposed to solve this situation with the use of a decreasing function in the regularization term, as previously proposed in [8] and [9].

In the present work, we study an energy functional to calculate the optical flow adding this operation in the smoothness term. We will see that it effectively reduces the rounded effects at the flow edges but the results are not so evident as expected. The parameters must be chosen carefully in order to avoid a degradation of the motion fields.

In the experimental results we will deal with two different kind of experiments: on the one hand, we will make a comparison between the best flows of the original and the new method, to observe the effect at the contours; on the other hand,

we will see the average error evolution with respect to the parameters of the new model for some standard synthetic sequences. Based on these results, we observe that, although the improvement is very positive in some sequences, it is not good enough in other experiments.

In Sect. 2, we explain the method and derive the numerical scheme that we have implemented. In Sect. 3 we show the experimental results and, finally, the conclusions in Sect. 4.

## 2 The Method

Given a set of images, $I : \Omega \subset \mathbb{R}^3 \to \mathbb{R}$, of gray values in space and time, $\mathbf{x} = (x, y, t)^T \in \Omega$, we define the motion field as $\mathbf{w} = (u(\mathbf{x}), v(\mathbf{x}), 1)^T$, being $u(\mathbf{x})$ and $v(\mathbf{x})$ the $x$ and $y$ displacements, respectively. We use $\nabla I = (I_x, I_y)^T$ to denote the spatial gradient of the image, with $I_x$, $I_y$ as the first order derivatives in $x$ and $y$. In general, we assume that the image intensities remain constant through the sequence, so the relation $I(\mathbf{x} + \mathbf{w}) - I(\mathbf{x}) = 0$ holds for the objects in the images. Our energy functional is as follows:

$$E(\mathbf{w}) = \int_\Omega \Psi\left((I(\mathbf{x}+\mathbf{w}) - I(\mathbf{x}))^2\right) \mathbf{dx} + \gamma \int_\Omega \Psi\left(|\nabla I(\mathbf{x}+\mathbf{w}) - \nabla I(\mathbf{x})|^2\right) \mathbf{dx} + \alpha \int_\Omega \Phi\left(|\nabla u|^2 + |\nabla v|^2\right) \mathbf{dx}. \tag{1}$$

with $\Psi\left(s^2\right) = \sqrt{s^2 + \epsilon^2}$ and $\Phi\left(s^2\right) = e^{-\lambda \|\nabla I\|^\kappa} \cdot \Psi\left(s^2\right)$.

When minimizing this energy, the associated Euler-Lagrange equations yield a system of reaction-diffusion PDEs. The diffusion process allows to fill the information in homogeneus regions, but it also smoothes the flow at the discontinuities. For this reason, we introduce a decreasing function, $e^{-\lambda \|\nabla I\|^\kappa}$, in the smoothness term, in order to reduce the regularization at flow edges. The Euler-Lagrange equations are given by the following expressions:

$$\begin{aligned} 0 =& \Psi'_D \cdot (I(\mathbf{x}+\mathbf{w}) - I(\mathbf{x})) \cdot I_x(\mathbf{x}+\mathbf{w}) \\ &+ \gamma\, \Psi'_G \cdot ((I_x(\mathbf{x}+\mathbf{w}) - I_x(\mathbf{x})) \cdot I_{xx}(\mathbf{x}+\mathbf{w}) \\ &+ (I_y(\mathbf{x}+\mathbf{w}) - I_y(\mathbf{x})) \cdot I_{xy}(\mathbf{x}+\mathbf{w})) - \alpha \operatorname{div}\left(\Phi'_S \cdot \nabla u\right), \end{aligned}$$

$$\begin{aligned} 0 =& \Psi'_D \cdot (I(\mathbf{x}+\mathbf{w}) - I(\mathbf{x})) \cdot I_y(\mathbf{x}+\mathbf{w}) \\ &+ \gamma\, \Psi'_G \cdot ((I_x(\mathbf{x}+\mathbf{w}) - I_x(\mathbf{x})) \cdot I_{xy}(\mathbf{x}+\mathbf{w}) \\ &+ (I_y(\mathbf{x}+\mathbf{w}) - I_y(\mathbf{x})) \cdot I_{yy}(\mathbf{x}+\mathbf{w})) - \alpha \operatorname{div}(\Phi'_S \cdot \nabla v), \end{aligned} \tag{2}$$

with $\Psi'(s^2) = \frac{1}{2\sqrt{s^2+\varepsilon^2}}$ and $\Phi'(s^2) = \frac{e^{-\lambda \|\nabla I\|^\kappa}}{2\sqrt{s^2+\varepsilon^2}}$.

In order to simplify the equations, we use the following notation:

$$\begin{aligned}\Psi'_D :=& \Psi'\left(\left(I(\mathbf{x}+\mathbf{w})-I(\mathbf{x})\right)^2\right),\\ \Psi'_G :=& \Psi'\left(\left|\nabla I(\mathbf{x}+\mathbf{w})-\nabla I(\mathbf{x})\right|^2\right),\\ \Phi'_S :=& \Phi'\left(|\nabla u|^2+|\nabla v|^2\right).\end{aligned} \tag{3}$$

The above equations are nonlinear because of the argument $\mathbf{w}$ and the functions $\Psi'$ and $\Phi'$; so, in order to linearize the equations, we follow the same strategy used in [3] and [7], enclosing our numerical scheme in two fixed point iterations. We introduce a first index, $n$, to remove the nonlinearity in $\mathbf{w}$, using the following first order Taylor expansions:

$$\begin{aligned}I(\mathbf{x}+\mathbf{w}^{n+1}) \approx& I(\mathbf{x}+\mathbf{w}^n)+I_x(\mathbf{x}+\mathbf{w}^n)du^n+I_y(\mathbf{x}+\mathbf{w}^n)dv^n\\ I_x(\mathbf{x}+\mathbf{w}^{n+1}) \approx& I_x(\mathbf{x}+\mathbf{w}^n)+I_{xx}(\mathbf{x}+\mathbf{w}^n)du^n+I_{xy}(\mathbf{x}+\mathbf{w}^n)dv^n\\ I_y(\mathbf{x}+\mathbf{w}^{n+1}) \approx& I_y(\mathbf{x}+\mathbf{w}^n)+I_{xy}(\mathbf{x}+\mathbf{w}^n)du^n+I_{yy}(\mathbf{x}+\mathbf{w}^n)dv^n,\end{aligned} \tag{4}$$

As proposed in [3], we work with the *motion increments* $(du^n, dv^n)$, so the optical flow can be iteratively estimated as $u^{n+1}=u^n+du^n$ and $v^{n+1}=v^n+dv^n$. We introduce a second index, $m$, that accounts for the nonlinearities of the $\Psi'$ and $\Phi'$ functions. Combining both fixed point schemes, the system of equations reads as:

$$\begin{aligned}0 =& (\Psi'_D)^{n,m}\cdot\left(I(\mathbf{y})+I_x(\mathbf{y})du^{n,m+1}+I_y(\mathbf{y})dv^{n,m+1}-I(\mathbf{x})\right)\cdot I_x(\mathbf{y})\\ &+\gamma\,(\Psi'_G)^{n,m}\cdot\Big(\left(I_x(\mathbf{y})+I_{xx}(\mathbf{y})du^{n,m+1}+I_{xy}(\mathbf{y})dv^{n,m+1}-I_x(\mathbf{x})\right)\cdot I_{xx}(\mathbf{y})\\ &\quad+\left(I_y(\mathbf{y})+I_{xy}(\mathbf{y})du^{n,m+1}+I_{yy}(\mathbf{y})dv^{n,m+1}-I_y(\mathbf{x})\right)\cdot I_{xy}(\mathbf{y}^{n,m})\Big)\\ &-\alpha\,\mathrm{div}\left((\Phi'_S)^{n,m}\cdot\nabla(u^{n,m}+du^{n,m+1})\right)\\ 0 =& (\Psi'_D)^{n,m}\cdot\left(I(\mathbf{y})+I_x(\mathbf{y})du^{n,m+1}+I_y(\mathbf{y})dv^{n,m+1}-I(\mathbf{x})\right)\cdot I_x(\mathbf{y})\\ &+\gamma\,(\Psi'_G)^{n,m}\cdot\Big(\left(I_x(\mathbf{y})+I_{xx}(\mathbf{y})du^{n,m+1}+I_{xy}(\mathbf{y})dv^{n,m+1}-I_x(\mathbf{x})\right)\cdot I_{xx}(\mathbf{y})\\ &\quad+\left(I_y(\mathbf{y})+I_{xy}(\mathbf{y})du^{n,m+1}+I_{yy}(\mathbf{y})dv^{n,m+1}-I_y(\mathbf{x})\right)\cdot I_{xy}(\mathbf{y}^{n,m})\Big)\\ &-\alpha\,\mathrm{div}\left((\Phi'_S)^{n,m}\cdot\nabla(v^{n,m}+dv^{n,m+1})\right),\end{aligned} \tag{5}$$

with $\mathbf{y}=\mathbf{x}+\mathbf{w}^{n,m}$.

This system of equations is solved by means of the SOR method and embeded in a pyramidal structure to allow detecting large displacements. Details on the implementation can be found in [7].

## 3 Experimental Results

In this section, we evaluate the method using some standard image sequences. In particular, we use some images from the Middlebury benchmark database and other synthetic images. The optical flows are represented using the same color scheme as in [7].

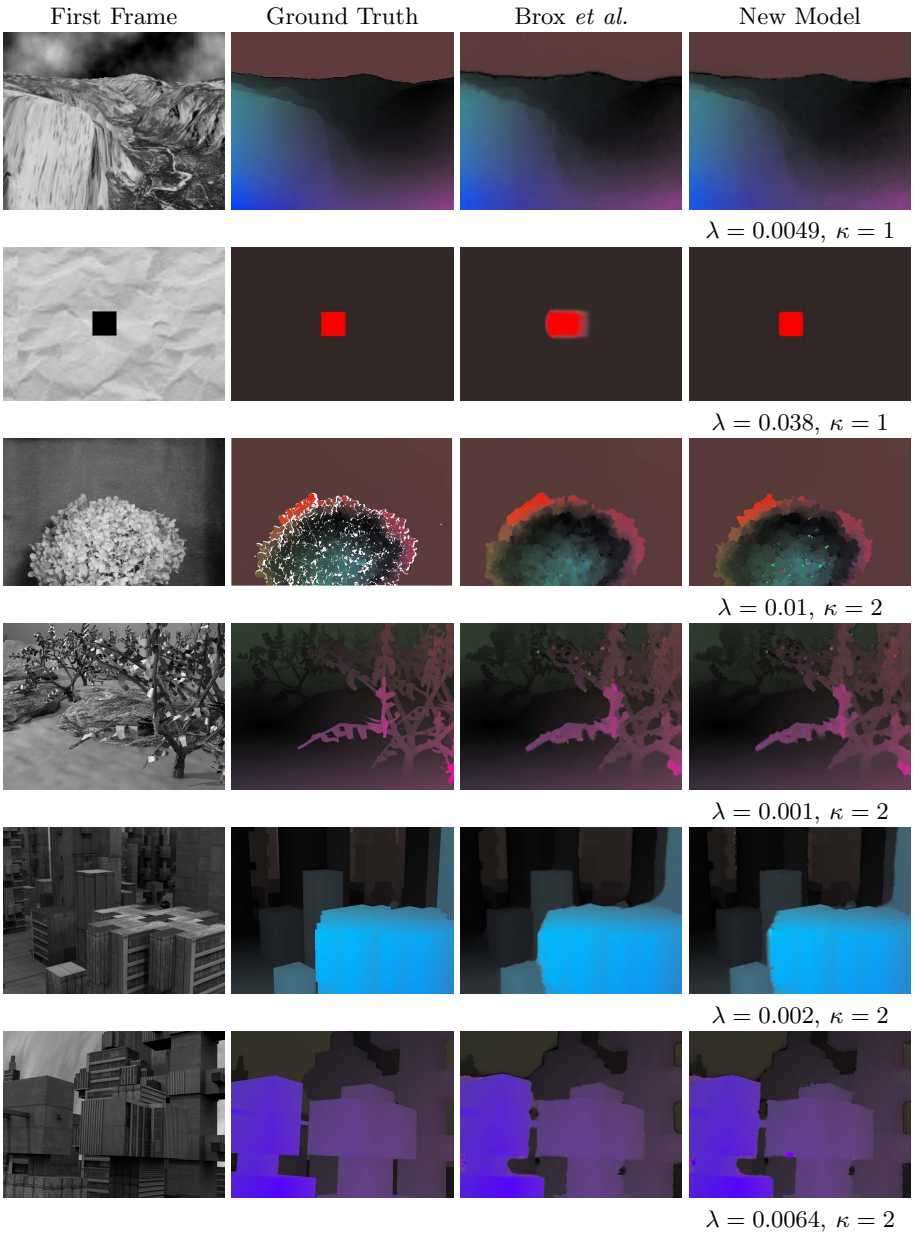


**Fig. 1.** Results for the Yosemite, Square, Hydrangea, Grove3, Urban2 and Urban3 sequences: In the first column, the image sequence; in the second column, the ground truth; in the third column, the result given by [7]; and, in the fourth column, the result given by (5)

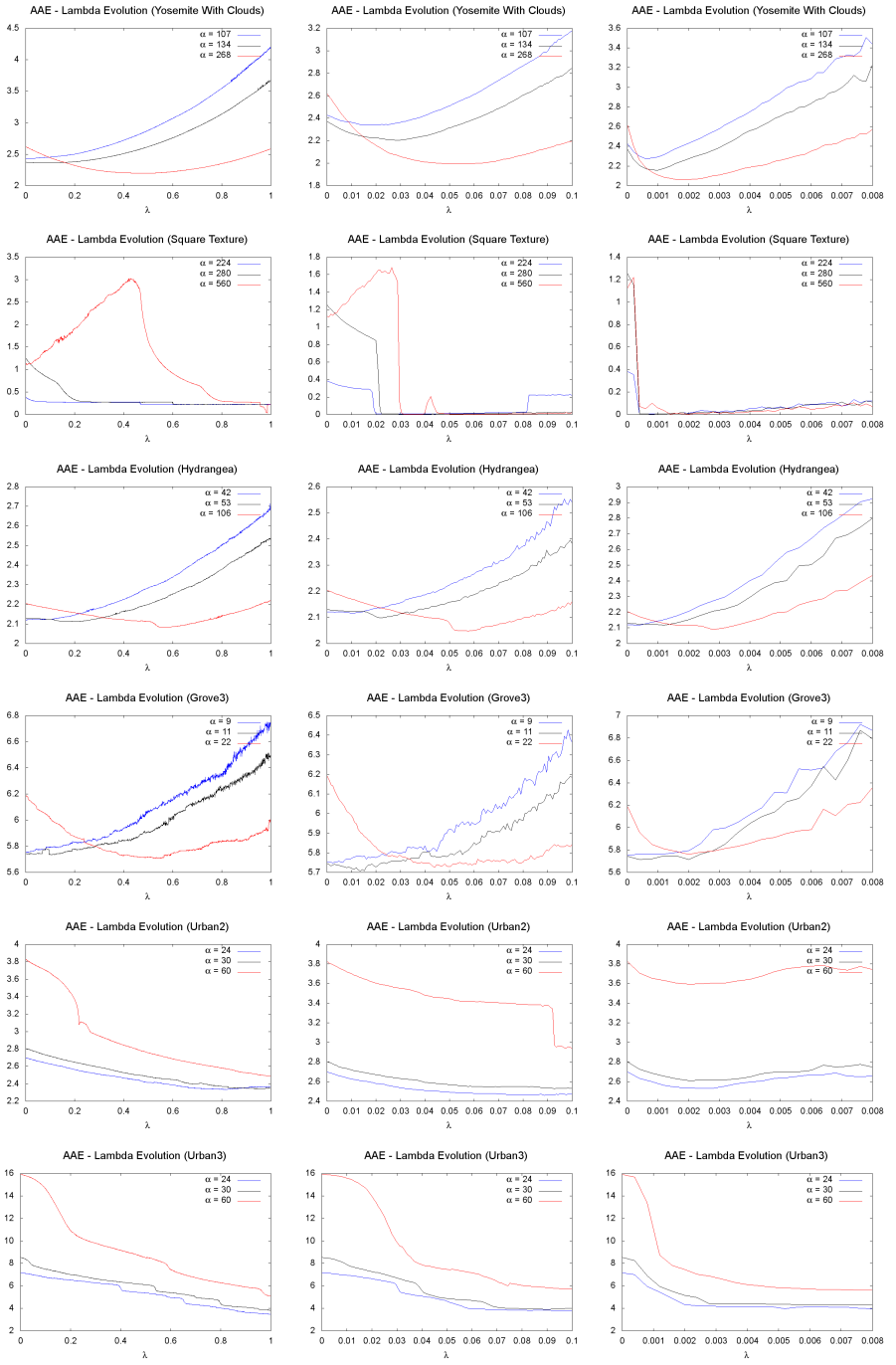


**Fig. 2.** Each row depicts the AAE for the sequences using different values of $\kappa$: 0.2 in the first column, 1 in the second and 2 in the third

In Fig. 1, we show the first frame of the sequences at the first column, their corresponding ground truths at the second, the best solutions of the original implementation at the third and, finally, the best solution for the new implementation. The first row depicts the yosemite sequence. We see that the flow is better than the original model, especially at the left mountain and in the separation between the sky and the mountains.

The second row shows a Square sequence, which reaches a very precise solution at the contours of the square. This solution is very close to the ground truth, highly improving the best result provided by Brox *et al.* This experiment shows that the method with the decreasing function can provide very good solutions for this kind of sequences.

Furthermore, the third row depicts a perfect example on discontinuity preserving that can be obtained using the new approximation. We notice that, despite some problematic areas on the flow, the contour detection is very close to the ground truth in Hydrangea. On the contrary, we observe some misleading flows inside the flower, which are probably due to a high value of the image gradient. The regularization term vanishes in these cases, so there appears outliers in the flow field. This problematic areas could be solved by adding a small constant value together with the decreasing function, so that it avoids removing the smoothing process.

The fourth and fifth rows show the results for Urban2 and Urban3 sequences respectively. We see how the exponential favours the contours detection in the buildings in both sequences, especially in Urban2.

In Fig. 2, we compare the Average Angular Error (AAE) evolution for the Yosemite, Square, Hydrangea, Grove3, Urban2 and Urban3 sequences with respect to the $\lambda$ parameter. We observe that, typically, when $\lambda$ increases, the AAE improves and the method provides better results, even for higher values of the smoothness parameter. In particular, the results for the Square sequence are surprising since, although $\lambda$ initially worsen the errors for a large $\alpha$, it abruptly attains very good results. On the other hand, when $\kappa$ increases, the value of $\lambda$ must decrease to achieve an optimal solution. In the case of Yosemite, the results are much more stable with respect to $\lambda$ and $\kappa$ parameters than the other graphics. On the other hand, the graphics for Urban2 and Urban3 are more unstable, which is probably due to the small values of $\alpha$.

## 4 Conclusions

In this paper, we have dealt with the problem of discontinuity preserving in optical flow. We have implemented a simple strategy to reduce the rounded effects that usually appear at the contours of the flow fields in TV-$L^1$ optical flow methods.

The expected result was that the decreasing function would enhance edge detection but, although this actually happened in some sequences, it has been less important than it was expected. The way the discontinuities are preserved depends strongly on the value of the $\lambda$ and $\kappa$ parameters: it is difficult to find

unique values that work fine for every image sequence. We have also observed that the method works fine in circumstances where the decreasing function does not cancel the regularization term. When this happens, it considerably increases the errors as we have seen in the experimental results. This problem could be solved by adding a modification to the method that prevents the cancellation of the decreasing function.

In a future work, we will examine this idea in depth. We will also study other strategies for the preservation of discontinuities like, for intance, the use of diffusion tensors in the smoothness term.

**Acknowledgment.** This work has been partially supported by the Spanish Ministry of Science and Innovation through the research project TIN2011-25488.

## References

1. Álvarez, L., Esclarín, J., Lefébure, M., Sánchez, J.: A pde model for computing the optical flow. In: XVI Congreso de Ecuaciones Diferenciales y Aplicaciones, C.E.D.Y.A. XVI, Las Palmas de Gran Canaria, Spain, pp. 1349–1356 (1999)
2. Baker, S., Scharstein, D., Lewis, J.P., Roth, S., Black, M.J., Szeliski, R.: A database and evaluation methodology for optical flow. International Journal of Computer Vision 92(1), 1–31 (2011)
3. Brox, T., Bruhn, A., Papenberg, N., Weickert, J.: High accuracy optical flow estimation based on a theory for warping. In: Pajdla, T., Matas, J(G.) (eds.) ECCV 2004. LNCS, vol. 3024, pp. 25–36. Springer, Heidelberg (2004)
4. Horn, B.K.P., Schunck, B.G.: Determining optical flow. Artificial Intelligence 17, 185–203 (1981)
5. Nagel, H.H., Enkelmann, W.: An investigation of smoothness constraints for the estimation of displacement vector fields from image sequences. IEEE Transanctions on Pattern Analysis and Machine Intelligence 8, 565–593 (1986)
6. Perona, P., Malick, J.: Scale-space and edge detection using anisotropic diffusion. IEEE Transactions on Pattern Analasys and Machine Intelligence 12, 629–629 (1990)
7. Sánchez, J., Monzón, N., Salgado, A.: Robust Optical Flow Estimation. Image Processing On Line 2013, 242–260 (2013)
8. Wedel, A., Cremers, D., Pock, T., Bischof, H.: Structure- and motion-adaptive regularization for high accuracy optic flow. In: IEEE International Conference on Computer Vision, pp. 1663–1668 (September 2009)
9. Xu, L., Jia, J., Matsushita, Y.: Motion detail preserving optical flow estimation. In: IEEE Conference on Computer Vision and Pattern Recognition (CVPR), pp. 1293–1300 (June 2010)
10. Zach, C., Pock, T., Bischof, H.: A Duality Based Approach for Realtime TV-$L^1$ Optical Flow. In: Hamprecht, F.A., Schnörr, C., Jähne, B. (eds.) DAGM 2007. LNCS, vol. 4713, pp. 214–223. Springer, Heidelberg (2007)